Mechanics of Advanced Composite Structures 10 (2023) 271 – 282

Semnan University

Mechanics of Advanced Composite Structures

journal homepage: http://MACS.journals.semnan.ac.ir

Stress Analysis of the Rotating Carbon-Carbon Composite Disk of an Axial Compressor

B. Shahriari*, K. Shojaei

Faculty of Mechanics, Malek Ashtar University of Technology, Isfahan, Iran.

KEYWORDS

Axial compressor;
Rotating disk;
Carbon-Carbon composite;
Mechanical stress;
Thermal stress.

ABSTRACT

The correct materials selection in the design of aerospace structures reduces the weight and increases structural efficiency. Since the rotor in gas turbine engines has a significant weight, it is important to reduce its weight. The rotating disks in these rotors are subjected to mechanical and thermal loads and experience high-temperature gradients and angular velocities. This work aims to analyze the stress of a rotating disk made of carbon-carbon (C/C) composite to withstand mechanical and thermal loads and reduce the weight of the rotor. The behavior of constant thickness C/C composite disks is studied based on the Tsai-Wu Failure Theory. To do so, first, the basic properties of the material, disk size, rotation speed, temperature distribution, and other requirements are determined. The differential governing equations are obtained by assuming the plane stress state, Hooke's law, and compatibility condition, and the stresses, strains, and displacements are obtained. Considering the safety factors of 1 and 1.5, the critical velocities are calculated using the Tsai-Wu failure theory. Finally, according to the information obtained from the analysis, the evaluation of disks with different layers is compared with other similar disks made with different materials.

1. Introduction

Rotating equipment, such as rotating disks, play a significant role in various industries, i.e., aerospace, automotive, and marine so it is important to do extensive investigations on their different aspects. In addition, rotating disks may experience different thermomechanical loading conditions makes studying their response of great importance. Rotating disks are vastly utilized in air engines, i.e., turbojets, mini turbojets, and turbofans, as a support for the blades of turbines and compressors. Engine structures, like other engineering structures, are built to meet required needs and always are constrained by design and performance limitations. Reducing the weight of an engine increases the overall efficiency and reduces the existing limitations and costs. Since the disks of an engine constitute a high portion of its weight, reducing their weight might enhance the performance. In this regard, researchers have presented new designs using optimization approaches and new materials to fulfill the strength-to-weight ratio needs. With the advent of low-weight and high-efficiency composites, attempts for optimizing the geometry and physical properties of rotating disks have been significantly increased. The availability of carbon fibers led to the development of improved materials now known as carbon-carbon (C/C) composites. The C/C composites consist of carbon fibers and carbon matrices. The attractive properties of carbon are combined with the high strength, versatility, and toughness of composites. The C/C composites were developed for elevated-temperature aerospace applications such as nose cones and rocket nozzles. These composites can be tailored to higher strengths and stiffness than other engineering metallic alloys and, unlike metals, can maintain these properties to high temperatures as indicated in Figure 1.

The fabrication costs for C/C composites are high and this has limited their use to primarily aerospace and military applications at present. Therefore, a reduction in costs will be achieved by an improvement in the carbon yield.

* Corresponding author. Tel.: +98-9131254280; Fax: +98-31-45227136
E-mail address: shahriari@mut-es.ac.ir

DOI: 10.22075/macs.2023.26800.1390
Received 2022-05-30 ; Received in revised form 2023-01-06 ; Accepted 2023-01-10.

Something like 63% by volume of the carbon-carbon produced in the world is used in aircraft braking systems [1]. The C/C brake materials were originally developed by the Super Temp Division of B. F. Goodrich Inc. in the USA. It is now commercially advantageous to employ C/C brakes on civil subsonic aircraft. Furthermore, the use of C/C has been exploited or postulated for some land vehicles such as racing cars (Figure 2), high-speed trains, and even main battle tanks (MBTs). Orthogonally woven 3-D carbon-carbon has been successfully employed in rocket throat manufacture of small radius and rocket motor 2-D C/C exit cone assembly for many years (Figure 3).

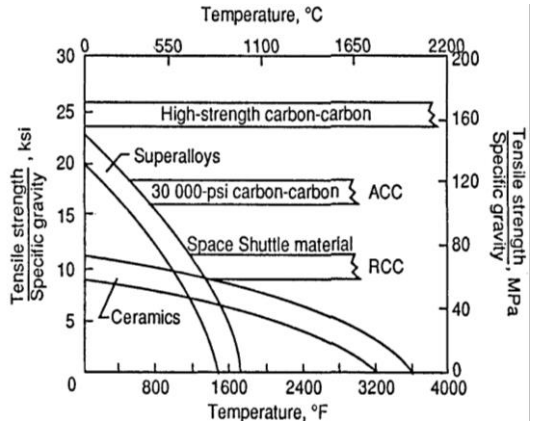

Fig.1. Strength-to-density ratio for several classes of high-temperature materials [2]

Fig.2. Carbon disk clutch system of a Formula1 racing car [1]

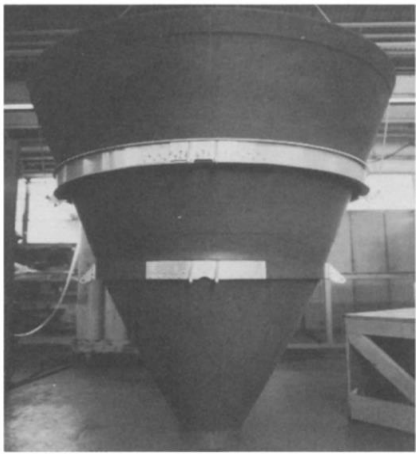

Fig.3. Rocket motor 2-D CC exit cone assembly [2]

Approximately 30 years ago, C/C composite was developed to meet the anticipated needs of the emerging space programs for materials that were resistant to high temperatures and were able to maintain structural integrity while experiencing the thermal stresses of reentry from space. The utility of this material was first demonstrated in a major Space Shuttle application where it was performed on the wing leading edge and nose cap thermal protection system. C/C technology has matured considerably since the first Space Shuttle application. Although more advanced versions continue to perform well on the Space Shuttle, C/C has evolved as a versatile material for a wide variety of new applications. The extreme thermomechanical requirements of the Space Shuttle have been the impetus for evaluating the properties of low-density CC. The use of CC on the nose cap and leading edges of the Space Shuttle makes it imperative to know as much as possible about all the characteristics of this material (Figure 4).

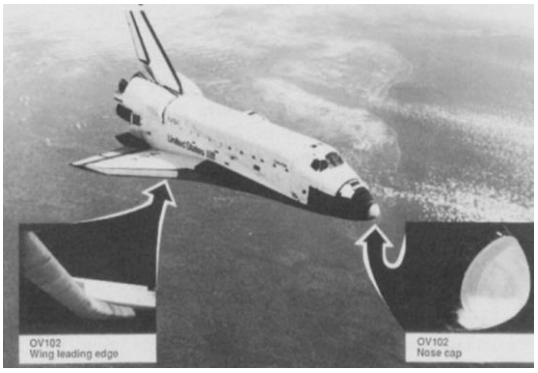

Fig.4. C/C areas on Space Shuttle arbiter [2]

Rotating disks used in gas turbine engines are commonly used at high angular velocities and experience high stresses. Accordingly, determining the stress and displacement fields is considered a serious purpose in the design of these structures. Stress analysis of these components has a long research history and has been an important topic in engineering design. Manson [3] proposed a finite difference method for calculating elliptic stress in gas turbine disks. This method can take into account changes in material properties, thickness as well as temperature. Millenson and Manson [4] developed this method to take into account the effects of plastic flow and creep. Both of these methods are widely used in industry today. Genta [5] modified the method proposed by Manson to be used in orthotropic materials. Timoshenko and Goodier [6] three-dimensionally analyzed a constant-thickness, isotropic disk. Using the semi-graphical method, Leopold [7] obtained the stress distribution on a disk of variable thickness. Lekhnitskii [8], Reddy and Srinath [9],

Gurushankar [10], Christensen and Wu [11], and Genta and Gola [12] were able to determine the stresses within orthotropic single-ply circular plates with stress-free outer boundaries, based on the theory of elasticity.

Parkes [13] proposed a general solution for obtaining thermal stresses in solid disks or anisotropic hollow disks exposed to symmetrical temperature rise. Foral and Newhouse [14] examined the performance of hoop-wound composite flywheel rotors. In this study, the energy stored criteria per unit swept volume, per unit rotor weight, and per unit material cost were used to evaluate the performance. After reviewing and designing many rotors, they eventually proposed the simple hoop wound rotor as a rotor easy to fabricate. Also, they presented a design approach that took into account the effect of different materials. In this study, it was shown that considering the effect of different materials can lead to increased energy storage. Tutuncu [15] in a study investigated the stress and deformation of rotating orthotropic circular plates under centrifugal force. In this study, the symmetric cross-ply and balanced laminates were investigated. However, the results of the paper show that the displacement in these problems is a function of radial coordinates. Kogo et al. [16] obtained the critical speed of C/C composite rotating disks with cracks.

Jain et al. [17] in one study, composite disks with uniform strength were examined. In this study, a method for designing such disks was proposed. In their study, the results obtained from the analytical solution were compared with the results of the finite element method analysis. Arnold et al. [18] analyzed a rotating disk as plane stress. The analytical model presented by them could analyze the rotor structure for surface tractions, body forces, and interfacial misfits. In this study, functional variables for disk design were presented. Sing and Ray [19] in one study investigated the creep effects on orthotropic aluminum-silicon carbide composite disks. In this study, the results obtained in this paper were compared with the results obtained from the Von Mises Yield Criterion.

To obtain a closed-form solution based on polynomials, Callioglu [20] investigated the thermal stress on an empty disk. For this purpose, a hollow disk was analyzed parabolically for thermal loading varying. In this study, the temperature on the inner surface of the disk was different from the outer surface of the disk. Koo [21] analyzed the disks for vibration. The critical velocity for the disks was also evaluated in this study. In this study, elastic stresses and fracture stresses were obtained for rotating cross-ply laminate disks. Callioglu et al. [22] proposed closed-form solutions to obtain the stress field in FGM disks that have a constant velocity. It was found that lower radial displacement is obtained by increasing elastic modulus from the inner radius to the outer one. On the other hand, the results of this paper show that by doing this correction, both radial and hoop stresses increase. Peng et al. [23] studied the elastic analysis of rotating functionally graded polar orthotropic disks. Zamaninezhad [24] obtained the exact solution of elastoplastic analysis of rotating disks made of functionally graded materials.

In a study, Zheng [25] examined stress and displacement in a functionally graded fiber-reinforced rotating disk. In this study, he considered angular thickness and velocity non-uniform. Zheng et al. [26] studied the stress field in functionally graded (FG) rotating disks with non-uniform thickness and variable angular velocity numerically. They assumed the elastic modulus and mass density of the disks to be varying along the radius as a power-law function of the radial coordinate, while Poisson's ratio is kept constant. The numerical results additionally reveal that deceleration results in shear-stress development within the disks where a greater deceleration leads to greater shear stress. Furthermore, the shear stress can cause a shift in the location of the maximum Von Mises stress, where for small deceleration, maximum Von Mises stress is located somewhere between the inner and outer radii, while for large deceleration it is located at the inner radius. The modal analysis of rotating annular disks was accomplished by Shahriari et al. [27] using the generalized differential quadrature method (GDQM).

Takkar et al. [28] studied the effect of polar and rectilinear orthotropic reinforcements, on rotating disk critical and bursting speeds, and stress distributions. They carried out Finite-element (FE) modeling of the disk using shell elements and determined the bursting by applying Tsai–Wu failure criteria. Shishesaz et al. [29] studied the thermoelastic behavior of a functionally graded nanodisk based on the strain gradient theory. They assumed that the nanodisk thickness is constant, and a power-law model is adopted to describe the variation of functionally graded material properties. Shahriari et al. [30] suggested a model in the framework of rotating a thick-walled hollow circular cylinder with free-clamp ends under centrifugal load for analysis of the compressors spool in a turbojet engine. Shahriari and Safari [31] applied four methods, variable material properties (VMP), Galerkin, and Runge-Kutta with two different rules to compute the amount of displacement, stress, and strain of a rotary functionally graded material (FGM) disk.

Farukoglu and Korkut [32] examined the elastic limit stresses and failure of a rotating variable thickness disk composed of fiber-reinforced material by utilizing the Tsai-Wu criterion. In another work, Farukoglu and Korkut [33] constructed an analytical approach to examine the limit stresses of a multilayered fiber-reinforced disk. Three different layer configurations are considered, which are decreasing, constant and increasing reinforcement from the inner to the outer radius of the disk. The multilayered disk is subjected to two boundary conditions, free-free and fixed-free. Wang et al. [34] presented the amplitude and vibrational characteristics of a rotating fiber metal laminated micro-disk. Kaur et al. [35] presented the effect of thermal and particle gradients in a rotating composite disk with variable thickness using Sherby's law. The values of tangential, radial stresses, and strain rates are calculated at different radii using mathematical modeling. It has been observed that with an increase in the variable thickness and particle gradient, the stresses and strain rates decrease, and determined that the creep deformation decreases with fluctuating thickness. Kaur and Gupta [36] investigated the effect of different particle sizes on a rotating composite disk in the presence of a thermal gradient. They used mathematical modeling to find the value of radial and tangential stress rates and strain rates.

This paper aims to examine a rotating disk made of carbon composite in two layers of radial and circumferential and two modes, with and without applying heat. Composite disks in different layers and the same thickness have been compared and the components of stress, strain, displacement, and their strength coefficients have been calculated. Also, the best layer of the laminate disk is shown according to the performance of the disk from the analysis. Figure 5 is a view of a type of layer of fibers in a disk, which is continuously repeated from the beginning to the end of the disk.

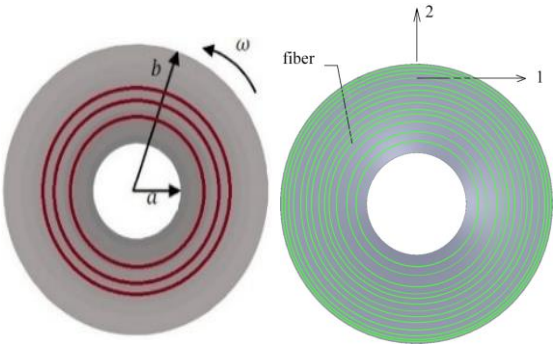

Fig. 5. A view of a type of layer of fibers in a disk

2. Governing Equations

A rotating annular disk made of radially reinforced composite material with an inner radius of a and an outer radius of b is shown in Figure 1. The disk is supposed to be large and thin enough rotates with the angular velocity of ω. Considering the effect of thickness-shear stress, the equilibrium equations of the rotating disk can be expressed by Eqs. (1) and (2)[37]:

$$\frac{\partial}{\partial_r}(\sigma_r.h.r)+\frac{\partial}{\partial_\theta}(\tau_{r\theta}.h)-\sigma_\theta h +\rho\omega^2 r^2 h=0 \tag{1}$$

$$\frac{\partial}{\partial r}(\tau_{r\theta}.h.r)+\frac{\partial}{\partial\theta}(\sigma_\theta.h)+\tau_{r\theta}h +\rho\dot{\omega}r^2 h=0 \tag{2}$$

where σ_r, σ_θ, and $\tau_{r\theta}$ are respectively the radial, circumferential, and shear stresses. Also, the radial and circumferential displacements are respectively denoted by u and v. Due to rotational symmetry and constant velocity, the strain-displacement relations are given by:

$$\varepsilon_r=\frac{du}{dr}\ ,\qquad \varepsilon_\theta=\frac{u}{r}\ ,\qquad \gamma_{r\theta}=0 \tag{3}$$

in which ε_r, ε_θ, and $\gamma_{r\theta}$ are radial, circumferential, and shear strains respectively. The strains can be generally related to the stresses and temperature gradients using the following equation:

$$\begin{bmatrix}\varepsilon_r\\ \varepsilon_\theta\\ \gamma_{r\theta}\end{bmatrix}=[S].\begin{bmatrix}\sigma_r\\ \sigma_\theta\\ \tau_{r\theta}\end{bmatrix}+T.\begin{bmatrix}\alpha_r\\ \alpha_\theta\\ 0\end{bmatrix} \tag{4}$$

where α_r, α_θ are thermal expansion coefficients in the r and θ directions and T is temperature, and $[S]$ the compliance matrix which can be expressed using Eq. (5):

$$[S]=\begin{bmatrix}\frac{1}{E_r} & \frac{-\nu_{\theta r}}{E_\theta} & 0\\ \frac{-\nu_{r\theta}}{E_r} & \frac{1}{E_\theta} & 0\\ 0 & 0 & \frac{1}{G_{r\theta}}\end{bmatrix} \tag{5}$$

For a homogeneous isotropic material $E_r=E_\theta$, $\nu_{r\theta}=\nu_{\theta r}$, and $\alpha_r=\alpha_\theta$. Substituting Eq. (5) into equation (4) and performing some simplifications, the stress components can be calculated as:

$$\sigma_r=\frac{E}{1-\nu^2}[(\varepsilon_r-\alpha T)+\nu(\varepsilon_\theta-\alpha T)]$$
$$\sigma_\theta=\frac{E}{1-\nu^2}[(\varepsilon_\theta-\alpha T)+\nu(\varepsilon_r-\alpha T)] \tag{6}$$

Taking the constant thickness into account, and substituting Eq (6) into Eq (1) yields:

$$\frac{d\sigma_r}{dr}+\frac{\sigma_r-\sigma_\theta}{r}+\rho\omega^2 r=0 \tag{7}$$

Substituting Eq (3) into Eq (7) and simplifications leads to the governing differential equation presented in Eq (8):

$$\frac{d^2u}{dr^2}+\frac{1}{r}\frac{du}{dr}-\frac{u}{r^2}=-\frac{(1-\nu^2)\rho\omega^2 r}{E} \tag{8}$$

The general exact solution of the above differential equation is in the form of Eq (9) [37]:

$$u_c=C_1 r+\frac{C_2}{r} \tag{9}$$

And the particular solution is obtained as follows:

$$u_p=-(1-\nu^2)\frac{\rho\omega^2 r^3}{8E} \tag{10}$$

Accordingly, the total displacement of the disk might be expressed by Eq. (11):

$$u=-\frac{\rho\omega^2 r^3(1-\nu^2)}{8E}+C_1 r+\frac{C_2}{r} \tag{11}$$

To calculate the constants, Eq. (6) is utilized in order to calculate the stresses as:

$$\begin{aligned}\sigma_r&=\frac{E}{1-\nu^2}\left[\frac{-(3+\nu)(1-\nu^2)\rho\omega^2 r^2}{8E}+(1+\nu)C_1-(1-\nu)\frac{C_2}{r^2}\right]\\ \sigma_\theta&=\frac{E}{1-\nu^2}\left[\frac{-(3+\nu)(1-\nu^2)\rho\omega^2 r^2}{8E}+(1+\nu)C_1+(1-\nu)\frac{C_2}{r^2}\right]\end{aligned} \tag{12}$$

Considering no tractions on the inner and outer surfaces of the disk, the radial stress is zero in the inner and outer radius, which results:

$$\begin{aligned}C_1&=\rho\omega^2\frac{(a^2+b^2)}{E}.\frac{(1-\nu)(3+\nu)}{8}\\ C_2&=\rho\omega^2\left(\frac{a^2.b^2}{E}\right).\frac{(1+\nu)(3+\nu)}{8}\end{aligned} \tag{13}$$

Substituting the constants into Eq. (12) and considering $\zeta=r/r_e$, $\beta=r_i/r_e$, and $\sigma_0=\rho\omega^2 r_e^2$:

$$\begin{aligned}\sigma_r&=\rho\omega^2 r_e^2 K_1\left(1+\beta^2-\frac{\beta^2}{\zeta^2}-\zeta^2\right)\\ \sigma_\theta&=\rho\omega^2 r_e^2\{K_1\left(1+\beta^2+\frac{\beta^2}{\zeta^2}\right)-K_2\zeta^2\}\\ \tau_{r\theta}&=0\end{aligned} \tag{14}$$

In this relation, the coefficients, K_1 and K_2, might be expressed as a function of the elements of the compliance matrix, as follows:

$$\begin{aligned}K_1&=\frac{2(S_{11}+S_{22})+S_{66}}{6(S_{11}+S_{22})+4S_{12}+2S_{66}}=\frac{3(S_{11}+S_{22})-2S_{12}}{8(S_{11}+S_{22})}\\ K_2&=\frac{S_{66}-4S_{12}}{6(S_{11}+S_{22})+4S_{12}+2S_{66}}=\frac{S_{11}+S_{22}-6S_{12}}{8(S_{11}+S_{22})}\end{aligned} \tag{15}$$

In this paper, due to the arrangement of the composites and the structure of the disks, governing equations should be rewritten in the cartesian coordinates system as Eq (16) [20]:

$$\begin{aligned}\frac{\partial\sigma_x}{\partial x}+\frac{\partial\tau_{xy}}{\partial y}-\frac{\partial U}{\partial x}&=0\\ \frac{\partial\tau_{xy}}{\partial x}+\frac{\partial\sigma_y}{\partial y}-\frac{\partial U}{\partial y}&=0\end{aligned} \tag{16}$$

where the potential function of body force, U, is given by the following formula:

$$U=-\frac{1}{2}\rho\omega^2(x^2+y^2) \tag{17}$$

The strain components concerning temperature and thermal expansion coefficients for a material are generally expressed by Eq. (18):

$$\begin{aligned}\varepsilon_x&=\frac{\partial u}{\partial x}=S_{11}\sigma_x+S_{12}\sigma_y+\alpha_x T\\ \varepsilon_y&=\frac{\partial v}{\partial y}=S_{12}\sigma_x+S_{22}\sigma_y+\alpha_y T\\ \gamma_{xy}&=\frac{\partial u}{\partial y}+\frac{\partial v}{\partial x}=S_{66}\tau_{xy}+\alpha_{xy}T\end{aligned} \tag{18}$$

In Eq. (18), α_x and α_y are respectively the thermal expansion coefficients in the x and y directions. In the Cartesian coordinate system, the compatibility equation states that:

$$\frac{\partial^2\varepsilon_x}{\partial y^2}+\frac{\partial^2\varepsilon_y}{\partial x^2}=\frac{\partial^2\gamma_{xy}}{\partial x\partial y} \tag{19}$$

Differentiating Eq. (16) with respect to x and y, yields.

$$\frac{\partial^2\tau_{xy}}{\partial x\partial y}=-\frac{1}{2}\left(\frac{\partial^2\sigma_x}{\partial x^2}+\frac{\partial^2\sigma_y}{\partial y^2}-\frac{\partial^2 U}{\partial x^2}-\frac{\partial^2 U}{\partial y^2}\right) \tag{20}$$

Using Eq. (20) in conjunction with Eqs. (18) and (19), the governing differential equation is obtained as:

$$s_{22}\frac{\partial^4 F}{\partial x^4}+(2s_{12}+s_{66})\frac{\partial^4 F}{\partial x^2\partial y^2}+s_{11}\frac{\partial^4 F}{\partial y^4}=-(s_{12}+s_{22})\frac{\partial^2 U}{\partial x^2}-(s_{11}+s_{12})\frac{\partial^2 U}{\partial y^2}-\alpha_x\frac{\partial^2 T}{\partial y^2}-\alpha_y\frac{\partial^2 T}{\partial x^2} \quad (21)$$

where F is the stress function that satisfies the following relations:

$$\sigma_x=\frac{\partial^2 F}{\partial y^2}+U,\quad \sigma_y=\frac{\partial^2 F}{\partial x^2}+U,\quad \tau_{xy}=-\frac{\partial^2 F}{\partial x\partial y} \quad (22)$$

Considering the temperature distribution function and body force, the solution of Eq. (21) for F is comprised of general and particular solutions. The particular solution might be expressed as:

$$F_1=D_1(x^2+y^2)^2 \quad (23)$$

where D_1 can be obtained by substitution of Eq (23) into Eq (21) as:

$$D_1=\frac{\rho\omega^2(s_{11}+2s_{12}+s_{22})}{24(s_{11}+s_{22})+8(2s_{12}+s_{66})}-\frac{T_m(\alpha_x+\alpha_y)}{[12(s_{11}+s_{22})+4(2s_{12}+s_{66})](b^2-a^2)} \quad (24)$$

in which T_m is the temperature difference in the inner and outer surfaces. The General solution for F might be calculated using Eq. (25):

$$\mathrm{F}_2=D_2(x^2+y^2)+D_3\ln(x^2+y^2) \quad (25)$$

The total stress function can be expressed as:

$$F=D_1(x^2+y^2)^2+D_2(x^2+y^2)+D_3\ln(x^2+y^2) \quad (26)$$

The constants D_2 and D_3 can be evaluated from the boundary conditions. The stress components are written as follows:

$$\sigma_x=4D_1(3y^2+x^2)+2D_2+2D_3\frac{x^2-y^2}{(x^2+y^2)^2}-\frac{1}{2}\rho\omega^2(x^2+y^2)$$

$$\sigma_y=4D_1(3x^2+y^2)+2D_2+2D_3\frac{y^2-x^2}{(x^2+y^2)^2}-\frac{1}{2}\rho\omega^2(x^2+y^2) \quad (27)$$

$$\tau_{xy}=4xy\left(-2D_1+\frac{D_3}{(x^2+y^2)^2}\right)$$

The stress components in cartesian coordinate can be transformed into their counterparts in the polar coordinate system using the following relations:

$$\sigma_r=\sigma_x m^2+\sigma_y n^2+2\tau_{xy}mn,\quad \sigma_\theta=\sigma_x n^2+\sigma_y m^2-2\tau_{xy}mn,\quad \tau_{r\theta}=-(\sigma_x-\sigma_y)mn+\tau_{xy}(m^2-n^2) \quad (28)$$

where $m=x/r$, $n=y/r$, and $r^2=x^2+y^2$. Introducing Eq. (27) into Eq. (28), the stress components in the polar coordinate system can be formulated as:

$$\sigma_r=4D_1r^2+2D_2+\frac{2D_3}{r^2}-\frac{1}{2}\rho\omega^2r^2,\quad \sigma_\theta=12D_1r^2+2D_2-\frac{2D_3}{r^2}-\frac{1}{2}\rho\omega^2r^2,\quad \tau_{r\theta}=0 \quad (29)$$

Considering zero radial stress at inner and outer radius, the following equations can be obtained for the sake of unknown coefficient, i.e., D_2 and D_3:

$$4D_1a^2+2D_2+\frac{2D_3}{a^2}-\frac{1}{2}\rho\omega^2a^2=0,\quad 4D_1b^2+2D_2+\frac{2D_3}{b^2}-\frac{1}{2}\rho\omega^2b^2=0 \quad (30)$$

which yields:

$$D_2=(-2D_1+\frac{1}{4}\rho\omega^2)(a^2+b^2),\quad D_3=(2D_1-\frac{1}{4}\rho\omega^2)a^2b^2 \quad (31)$$

In this study the temperature at the inner and outer radius is supposed to be 4300°C and 7000°C respectively, which varies as a quadratic function of radius as shown in Figure 6 and stated by Eq. (32):

$$T=T_m\frac{r^2-a^2}{b^2-a^2}+430 \quad (32)$$

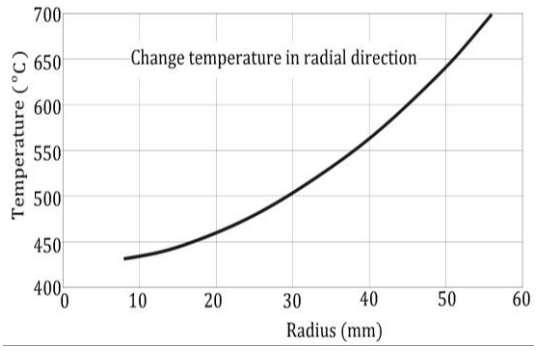

Fig. 6. Variation of temperature along the radius

The temperature function is entered as a quadratic function of the radius in the corresponding equations. It should also be noted that with every 1000 ℃ increase in temperature, the strength of carbon decreases by about 11% [38]. The change of mechanical and physical properties with temperature for each layer is discretely entered into the code and the function related to the changes of properties with temperature is extracted and included in the analysis.

3. Validation for Calculation of Circumferential and Radial Stresses

A Code was written for this research and compared with the basic reference [20] to evaluate. In the example given from reference [20], a glass-fiber/epoxy prepreg orthotropic rotating hollow disk is used in the solution. It is subjected to thermal loading that is varying parabolically from the inner surface to the outer surface along the radial section. The Mechanical properties of the composite material used in this reference are given in Table 1. In this example, the inner and outer radii are 40 and 100 mm respectively, and the density is 2.03 $e^{-6}kg/mm^3$, and the speed is 94.25 rad/s.

Table1. Mechanical properties of the composite material used in reference [20]

Mechanical properties		
Longitudinal elasticity modulus (MPa)	E_1	26950
Transverse elasticity modulus (MPa)	E_2	21800
Shear modulus (MPa)	G_{12}	7540
Poisson's ratio	ν_{12}	0.15
Thermal expansion coefficient (1/℃)	α_x	3.1×10^{-6}
Thermal expansion coefficient (1/℃)	α_y	5.5×10^{-6}

In this example, six different temperatures were used, 0, 50, 100, 150, 200, and 250°C and the material was investigated and analyzed. Figure 7 shows the circumferential stress and Figure 8 shows the radial stress in the solved example from reference [20].

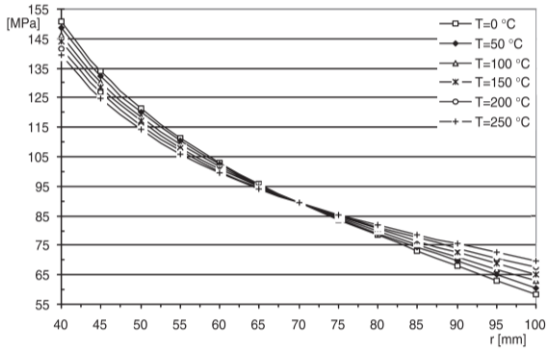

Fig.7. Distributions of the circumferential stress components along the radial section of the disk in reference [20]

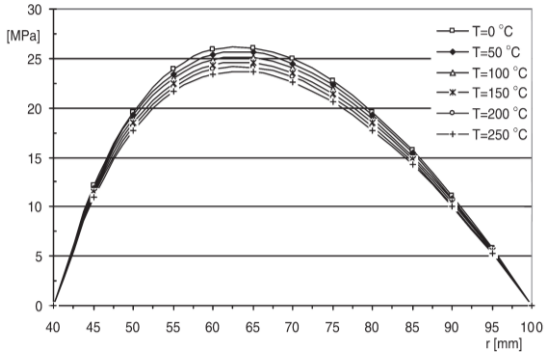

Fig. 8. Distributions of the radial stress components along the radial section of the disc in reference [20]

Figures 9 and 10 show respectively the circumferential stress and radial stress obtained from the code written in this research. The comparison of the stresses resulting from this research and reference [20] shows the validity of the analytical codes. As seen in these figures, when temperature is increased further, σ_θ decreases at the inner surface, whereas increases at the outer surface. The circumferential stress is found to be highest, 150.95 MPa, at the inner surface. σ_r is zero at both the inner and outer surfaces.

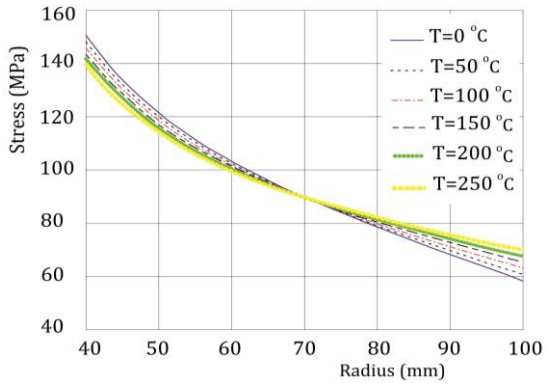

Fig.9. Distributions of the circumferential stress components along the radial section of the disk in this research

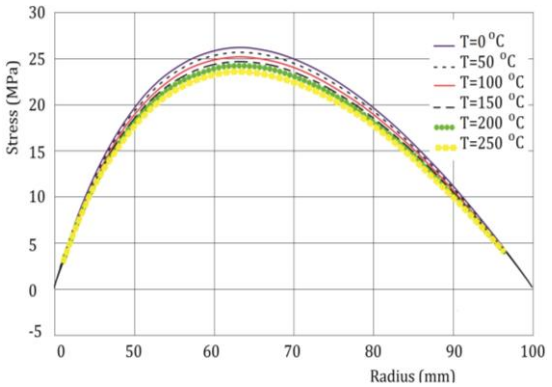

Fig. 10. Distributions of the radial stress components along the radial section of the disc in this research

4. Results and Discussions

In this paper, as shown in Figure 7, two kinds of fiber alignments, i.e., radial and circumferential, are considered. The materials parameters of the utilized composite material property of the material, the size of the disk, and the temperature are shown in Table 2. The loading condition as well as geometrical properties are presented in Table 3. The first letter in TC, TT, LC, and LT shows thickness and length, and the second letter shows compression and tensile in the composite.

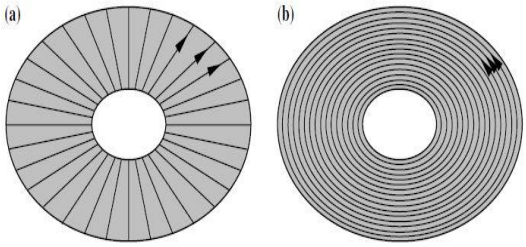

Fig. 11. (a) radially-reinforced and; (b) circumferentially-reinforced composite disks

Table 2. Property of composite used [38]

TC $(\sigma_2^c)_{ult}$ MPa	TT $(\sigma_2^t)_{ult}$ MPa	LC $(\sigma_1^c)_{ult}$ MPa	LT $(\sigma_1^t)_{ult}$ MPa
130	80	350	250
$(\tau)_{ult}$ MPa	α_2 $(10^{-6})1/C^0$	α_1 $(10^{-6})1/C^0$	υ_{12}
10	5	-0.3	0.41
G_{12} GPa	E_2 GPa	E_1 GPa	ρ
30	15	100	1800

Table 3. Property and size of disk used

T_i(°C)	T_o(°C)	ω(rad/s)
430	700	900
a=r_i(mm)	b=r_o(mm)	
8	56	

For the considered cases, the material constants should be assigned using Eqs. (33) and (34), respectively:

$$E_r = E_1, \qquad E_\theta = E_2, \qquad G_{r\theta} = G_{12}, \qquad \nu_{r\theta} = \nu_{12} \tag{33}$$

$$E_r = E_2, \qquad E_\theta = E_1, \qquad G_{r\theta} = G_{12}, \qquad \nu_{r\theta} = \nu_{21} \tag{34}$$

Equations (33) and (34) are respectively associated with radial and circumferential layouts. The radial displacement can then be calculated as $u = \varepsilon_\theta . r$. The radial and circumferential stresses of both layouts are identical, as can be perceived from Eqs. (33) and (14). Figure 12 shows the radial and circumferential stresses as a function of radius. Referring to this figure, the maximum radial and circumferential stresses without taking the thermal effects into account are 1.3014 MPa and 3.57 MPa respectively. Considering the thermal effects, these quantities are respectively 1.2258 MPa and 3.3703 MPa. It is worth noting that the maximum circumferential stresses in both states have happened at the inner radius of the disk.

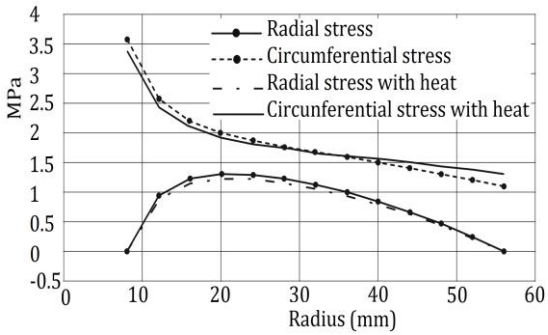

Fig. 12. The radial and circumferential stresses as a function of radius

The radial and circumferential strains of radial and circumferential layouts are respectively illustrated in Figures 13 and 14. The maximum values of radial and circumferential strains in radial layout and without taking the thermal effects into account are about 5.21×10^{-6} and 2.381×10^{-4} respectively. Considering the thermal effects, these quantities are about 4.7128×10^{-6} and 2.2469×10^{-4} respectively.

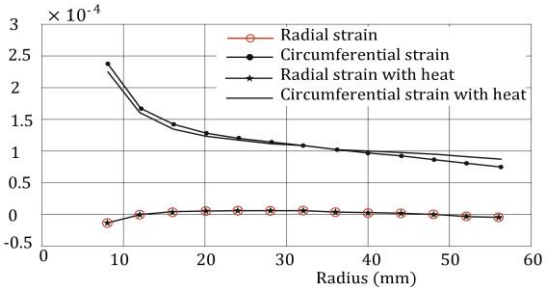

Fig. 13. Radial and circumferential strains in a radial layout

In circumferential layout, without taking the thermal effects into account, the maximum radial and circumferential strains are about 7.8558×10^{-5} and 3.5733×10^{-5} respectively. However, considering the thermal effects, these values are about 7.3861×10^{-5} and 3.3703×10^{-5} respectively.

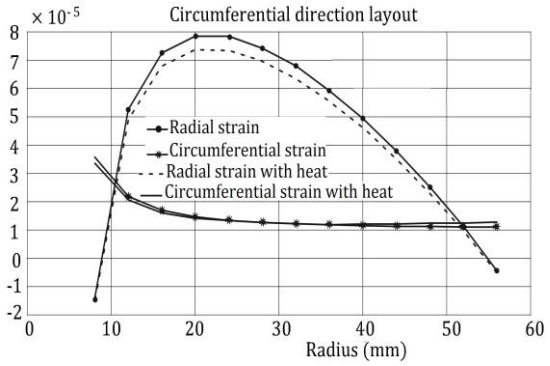

Fig. 14. Radial and circumferential strain in circumferential layout

The displacement distribution of radial and circumferential configurations is respectively depicted in Figures 15 and 16. The maximum displacement calculated in radial layout without thermal effects is about 4.1197 μm and by considering the thermal effects this value is about 4.8358 μm. However, the maximum displacement in circumferential layout with thermal effects is 0.612 μm, while without thermal effects is about 0.725 μm.

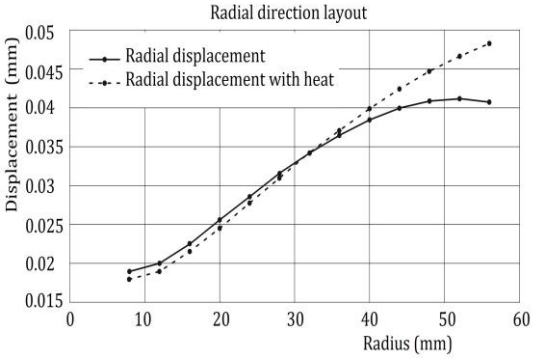

Fig. 15. Displacement in a radial layout

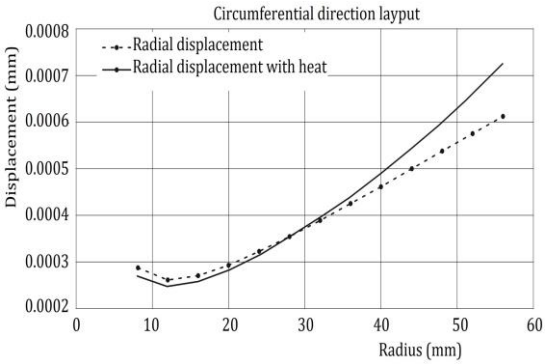

Fig. 16. Displacement in circumferential layout

5. Failure Theory

As mentioned earlier, the Tsai-Wu failure theory is utilized in order to find the velocity at which the disk may fail. Based on this theory, the following relation must be satisfied [38]:

$$H_1\sigma_1 + H_2\sigma_2 + H_6\tau_{12} + H_{11}\sigma_1^2 + H_{22}\sigma_2^2 + H_{66}\tau_{12}^2 + 2H_{12}\sigma_1\sigma_2 < 1 \quad (35)$$

in which H_1, H_2, H_6, H_{11}, H_{22}, H_{66}, and H_{12} are defined as follows:

$$H_1 = \frac{1}{(\sigma_1^T)_{ult}} - \frac{1}{(\sigma_1^C)_{ult}}$$

$$H_2 = \frac{1}{(\sigma_2^T)_{ult}} - \frac{1}{(\sigma_2^C)_{ult}}$$

$$H_6 = 0$$

$$H_{11} = \frac{1}{(\sigma_1^T)_{ult}\,(\sigma_1^C)_{ult}} \quad (36)$$

$$H_{22} = \frac{1}{(\sigma_2^T)_{ult}\,(\sigma_2^C)_{ult}}$$

$$H_{66} = \frac{1}{(\tau_{12})_{ult}^2}$$

$$H_{12} = -\frac{1}{2}\sqrt{\frac{1}{(\sigma_1^T)_{ult}(\sigma_1^C)_{ult}(\sigma_2^T)_{ult}(\sigma_2^C)_{ult}}}$$

In radial layout, according to the utilized fracture theory and without and with taking thermal effects into account, the lowest strength factor is obtained as 22.3945 and 22.075 respectively. Considering the safety factor of 1.5, the critical disk speed is obtained at about 3477 rad/s. However, for the safety factor of 1, this speed is about 4259 rad/s. When the thermal effects are taken into account, these values are obtained as 3452.6 rad/s and 4228 rad/s respectively.

For circumferential layout, without thermal effects, and the safety factor of 1.5 and 1, the critical speed is about 5786 rad/s and 7086rad/s respectively. These quantities are respectively calculated as 5744.6 rad/s and 7035 rad/s when the thermal effects are not neglected. It is worthwhile mentioning that in both layouts, the failure starts at the inner radius.

6. Advantages of Using Carbon Composites

In order to assess the benefits of using the disks fabricated from carbon composites over those produced from glass/epoxy [20], two disks

with the same size and volume are considered. In this case, the ratio of the mass is proportional to the ratio of their density: With consider the size of two disks can say that:

$$\frac{m_1}{m_2} = \frac{\rho_{c-c}}{\rho_{g-e}} = \frac{1800}{2030} = 0.8867 \quad (37)$$

in which ρ_{c-c} and ρ_{g-e} are the density of carbon and glass/epoxy composites respectively.

In addition, the strength coefficient ratio is obtained as:

$$\frac{SR_{c/c}}{SR_{g/e}} = \frac{22.39}{9.57} = 2.34 \quad (38)$$

According to what was mentioned above, although the mass of the carbon disk is less than the glass/epoxy one, the strength coefficient is higher.

7. Conclusion

The laminate layer has high performance with less displacement and less circumferential strain. The amount of circumferential strain in all layers is in accordance with the Eq. (6) equation $\varepsilon_\theta = S_{21}\sigma_r + S_{22}\sigma_\theta$ it will be counted. Since the values of radial and circumferential stresses and the S_{21} coefficient are equal in both layers, so the only difference in the circumferential strain of these two layers is in the S_{22} coefficient. This coefficient is related to E_θ and since this coefficient is higher in the peripheral layer therefore, it can be concluded that S_{22} is less in the peripheral stratification, which causes the circumferential strain to be less in the peripheral stratification, so this laminate layer has less displacement than the radial laminate layer, so a failure in this laminate occurs later. Due to the disks in compressor or turbine sections of gas turbine engines may not be geometrically axisymmetric, for example, they may have connection holes or Corrugated hubs, the structural analysis of the composite disk with asymmetric geometry is suggested. Also, the frequency analysis of the composite disk with thermal gradient, and the asymmetric geometry are interesting and practical topics for researchers.

References

[1] Savage, G., 1993. *Carbon-Carbon Composites*. Chapman & Hal.

[2] Buckley, J.D. and Edie, D.D., 1993. *Carbon–Carbon Materials and Composites.* Noyes Publications.

[3] Manson, S.S., 1947. *The determine of elastic stresses in gas-turbine disks*. No. NACA-TN-1279.

[4] Millenson, M.B. and Manson, S.S., 1948. *Determination of stresses in gas-turibe disks subjected to plastic flow and creep*. No. NACA-TN-1636.

[5] Genta, G., 1985. Kinetic energy storage; theory and practice of advanced flywheel system. Butterworths, London.

[6] Timoshenko, S.P. and Goodier, J.N., 1970. *Theory of elasticity*. McGraw-Hill.

[7] Leopold, W., 1948. Centrifugal and thermal stresses in rotating disks. *Applied Mechanics-Trasdactions of the ASME, 15*, pp. 322-326.

[8] Lekhnitskii, S., 1981. *Theory of elasticity of an anisotropic body*. Mir publisher.

[9] Reddy, T.Y. and Srinath, H., 1974. Elastic Stresses in a rotating anisotropic annular disk of variable thickness and variable density*. International Journal of Mechanical Sciences, 16(2)*, pp. 85-89.

[10] Gurushankar, G.V., 1975. Thermal stresses in a rotating nonhomogeneous, anisotropic disk of varying thickness and density. *Journal of Strain Analysis , 10(3),* pp. 137-142.

[11] Christensen, R.M., and Wu, E.M., 1977. Optimal design of anisotropic (fiber-reinforced) flywheels. *Journal of composite Materials, 11(4),* pp. 395-404.

[12] Genta, G., and Gola, M., 1981. The stress distrubtion in orthotropic rotating disks. *Applied Mechanics*, pp. 559-562.

[13] Parkes, E., 1976. Thermal stresses in anisotropic disks, *Int. J . Mech. Sci*, pp. 5-10.

[14] Foral, R.F., and Newhouse, N.L., 1980. On the performance of hoop wound composite flywheel rotors. *flywheel technology Symposium*, Scottsdle, AZ.

[15] Tutuncu, N., 1995. Effect of anisotropy on stresses in rotating disks. *International Journal of Mechanical Sciences, 37(8),* pp. 873-881.

[16] Kogo, Y., Hatta, H., Kawada, H., Shigemura, T., Ohnabe, H., Mizutani, T. and Tomioka, F., 1998. Spin burst test of carbon-carbon composite disk. *Journal of Composite Materials*, *32(11),* pp.1016-1035.

[17] Jain, R., Ramachandra, K. and Simha, K.R.Y., 1999. Rotating anisotropic disk of uniform strength. *Int. J. Mech. Sci*., *41(6),* pp. 639-648.

[18] Arnold, S.M., Saleeb, A.F. and Al-Zoubi, N.R., 2002. Deformation and life analysis of composite flywheel disk system. *Composite Part B: Engineering, 33(6),* pp. 433-459.

[19] Sing, S.B. and Ray, S., 2002. Modeling the anisotropy and creep in Orthotropic Aluminum-Silicon Carbide Composite rotating disk. *Mechanics of Material*, 34(6), pp. 363-372.

[20] Callioglu, H., 2004. Stress analysis of an orthotropic rotating disk under Thermal loading. *J. Reinforced Plastic and Composites, 23(17),* pp. 1859-1867.

[21] Koo, K.N., 2006. Vibration analysis and critical speeds of polar orthotropic annular disks in rotation*. Composite Structures, 76(1-2),* pp. 67-72.

[22] Callioglu, H., Bektas, N. B. and Sayer, M., 2011. Stress analysis of functionally graded rotating discs: analytical and numerical solutions. *Acta Mechanica Sinica, 27(6),* 950-955.

[23] Peng, X.L. and Li, X.F., 2012. Elastic analysis of rotating functionally graded polar orthotropic disks. *International Journal of Mechanical Sciences, 60(1),* 84-91.

[24] Zamaninejad, M., Rastgoo, A. and Hadi, A., 2014. Exact elasto-plastic analysis of rotating disks made of functionally graded materials. *International Journal of Engineering Science, 85*, 47-57.

[25] Zheng, Y., 2016. *Displacement and stress analysis of functionally graded fibre-reinforced disk with non-uniform thickness and angular velocity* (Master of Science thesis, Northeastern University, Boston, Massachusetts).

[26] Zheng, Y., Bahaloo, H., Mousanezhad, D., Mahdi, E., Vaziri, A. and Nayeb-Hashemi, H., 2016. Stress analysis in functionally graded rotating disks with non-uniform thickness and variable angular velocity, *International Journal of Mechanical Sciences*, *119*, pp. 283-293.

[27] Shahriari, B., Jalali, M. and Karamooz Ravari, M., 2017. Vibration analysis of a rotating variable thickness bladed disk for aircraft gas turbine engine using generalized differential quadrature method. *Proceedings of the Institution of Mechanical Engineers, Part G: Journal of Aerospace Engineering, 231(14),* pp.2739-2749.

[28] Takkar, S., Gupta, K., Tiwari, V. and Singh, S. P., 2019. Dynamics of Rotating Composite Disk. *J. Vib. Eng. Technol., 7(6),* pp. 629–637.

[29] Shishesaz, M., Hosseini, M., Naderan Tahan, K. and Hadi, A., 2017. Analysis of functionally graded nanodisks under thermoelastic loading based on the strain gradient theory. *Acta Mechanica*, *228 (12),* pp.4141-4168.

[30] Shahriari, B., Sadeghinezhad, M.S. and Yousefi, S., 2019. Thermoelastic analysis of compressor spool in turbojet engine and redesign it using functionally graded materials with opti-mal coefficients. *Mechanics of Advanced Composite Structures*, *6 (2),* pp.167-179.

[31] Shahriari, B. and Safari, M., 2020. Stress Analysis of FGM Rotating Disk Subjected to Mechanical and Thermal Loads in Aircraft Gas Turbine Engine. *Mechanics of Advanced Composite Structures, 7 (1),* pp.1-13.

[32] Farukoglu, O. C. and Korkut, I., 2021. On the elastic limit stresses and failure of rotating variable thickness fiber reinforced composite disk. *ZAMM-Journal of Applied Mathematics and Mechanics, 101(9),* e202000356.

[33] Farukoglu, O. C. and Korkut, I., 2021. Failure stress response of rotating multilayered fiber reinforced annular disk. *Mechanics Based Design of Structures and Machines*, 1-15.

[34] Wang, Z., Yu, S., Xiao, Z. and Habibi, M., 2022. Frequency and buckling responses of a high-speed rotating fiber metal laminated cantilevered microdisk. *Mechanics of Advanced Materials and Structures*, *29(10),* pp.1475-1488.

[35] Kaur, H., Gupta, N. and Jain, A., 2022. Creep in rotating composite disk having variable thickness subjected to thermal as well as particle gradient. *AIP Conference* Proceedings*. AIP Publishing LLC*, 2555(1), p. 040002.

[36] Kaur, H. and Gupta, N., 2022. The effect of different particle size on the rotating composite disk subjected to thermal gradient. *Journal of Algebraic Statistics*, *13(1),* pp.199-209.

[37] Vullo, V. and Vivio, F., 2013. *Rotors: Stress analysis and design.* Berlin: Springer.

[38] Morgan, P., 2005. *Carbon fibers and their composites*. CRC press.